General Disclaimer

One or more of the Following Statements may affect this Document

- This document has been reproduced from the best copy furnished by the organizational source. It is being released in the interest of making available as much information as possible.

- This document may contain data, which exceeds the sheet parameters. It was furnished in this condition by the organizational source and is the best copy available.

- This document may contain tone-on-tone or color graphs, charts and/or pictures, which have been reproduced in black and white.

- This document is paginated as submitted by the original source.

- Portions of this document are not fully legible due to the historical nature of some of the material. However, it is the best reproduction available from the original submission.

Produced by the NASA Center for Aerospace Information (CASI)

NASA TECHNICAL MEMORANDUM

NASA TM-73878

NASA TM-73878

(NASA-TM-73878) HIGH TEMPERATURE ENVIRONMENTAL EFFECTS ON METALS (NASA) 19 p HC A02/MF A01 CSCL 21E

N78-19158

Unclas

G3/07 08680

HIGH TEMPERATURE ENVIRONMENTAL EFFECTS ON METALS

by S. J. Grisaffe, C. E. Lowell, and C. A. Stearns
Lewis Research Center
Cleveland, Ohio 44135

TECHNICAL PAPER presented at the
Twenty-fourth Sagamore Army Materials Research Conference
"Risk and Failure Analysis for Reliability"
Bolton Landing, New York, August 22-26, 1977

MAR 1978
RECEIVED
NASA STI FACILITY

E-9484

HIGH TEMPERATURE ENVIRONMENTAL EFFECTS ON METALS

S. J. Grisaffe, C. E. Lowell, and C. A. Stearns

NASA-Lewis Research Center

Cleveland, Ohio 44135

INTRODUCTION

Propulsion and power generation systems require components that will function for extended periods of time under high temperatures and stresses in hostile environments. These components are designed primarily on the basis of mechanical properties such as strength, fatigue life and creep resistance (Ref. 1). With this type of design approach, for systems where the operating parameters of temperature, stress, etc. are well characterized, component life is often found to be controlled by environmental attack. The factors involved in environmental attack are not readily included in component design criteria because they are not sufficiently well defined or understood. This situation has made it difficult and risky to predict long time service behavior on the basis of results obtained in accelerated, well controlled laboratory tests. Furthermore, little reliable and systematic data are available on service failures and operational histories of components so there is no good base for making life prediction correlations.

This paper is an overview of present understanding and ability to predict high temperature environmental attack of metals. The gas turbine engine is used as an example but most of the technology applies equally to other systems.

ENVIRONMENTAL ATTACK IN A GAS TURBINE ENGINE

Environmental attack in a gas turbine engine derives from (1) high temperatures, (2) combustion products of the air and

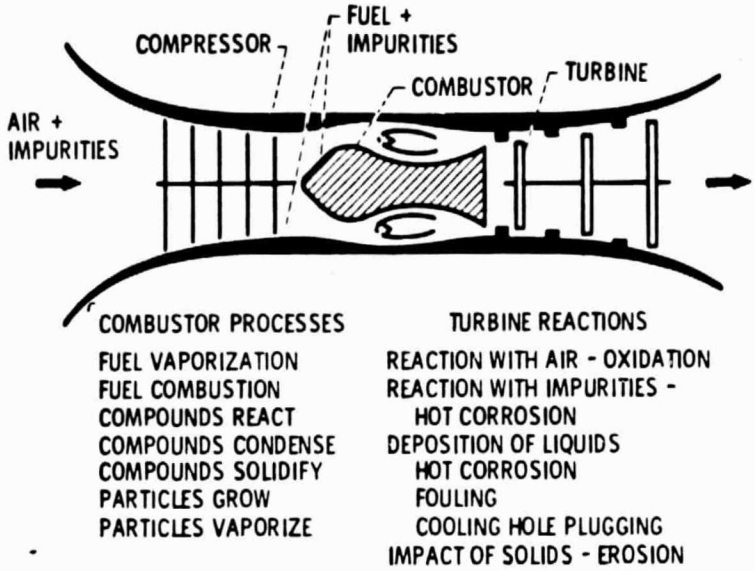

Figure 1. Origins of environmental attack in the hot section of a gas turbine engine.

fuel burned, and (3) impurities. The impurities enter the system with both the fuel and air as represented in figure 1. In the combustor where the fuel is burned, other physical and chemical processes also occur. The impurities can oxidize, vaporize, and react to form chemical compounds (Refs. 2, 3). Thus the hot combustion gases, which exit the combustor and enter the turbine, can contain a variety of potentially harmful constituents. Oxidation attack of hot-gas-path metallic components results from reaction with oxygen and oxides of carbon. Liquid and gaseous species can cause an accelerated type of oxidation attack called hot corrosion (Ref. 4). Airfoil cooling holes can be plugged and the turbine aerodynamic efficiency can be reduced by fouling as a result of deposition of materials from the combustion product gas flow (Ref. 5). Solid particles can impact components and produce erosion which both destroys optimum airfoil configurations and reduces load-bearing cross-sections (Ref. 6). All of these processes limit component life over a range of service temperatures as indicated very schematically in figure 2. Of course, it must be emphasized that the domains of the environmental attack life limits are variable depending on environmental conditions. Thus we see from figure 2 that while components are designed to rather well-defined fatigue and creep limits, environmental attack can result in very early failures.

ORIGINAL PAGE IS
OF POOR QUALITY

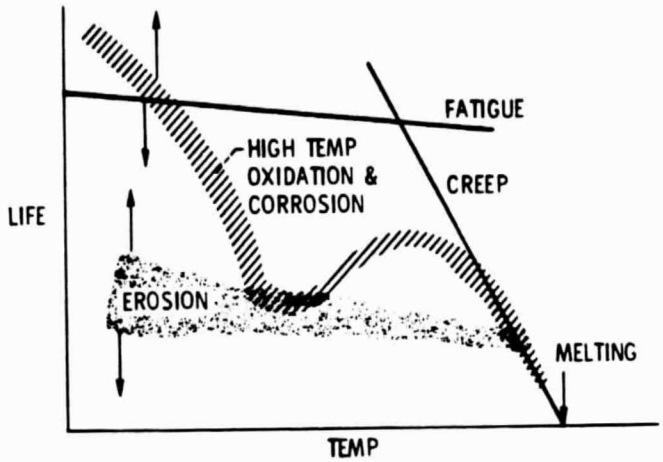

Figure 2. Schematic representation of turbine components life-limiting factors.

High Temperature Oxidation

Of all the modes of environmental attack, oxidation has been the most studied and is probably the best understood. Oxidation attack of metallic surfaces manifests itself in a number of different ways, some of which are depicted in figure 3. For a one component metal system, the oxidation reaction converts the surface to a single oxide scale which grows rapidly at first but slows to a low growth rate. The amount of oxide formed is a function of the particular metal, the temperature, and oxygen pressure. This type of oxidation behavior is characterized by a parabolic growth rate curve and involves only increases in weight resulting from oxygen pickup. Bulk diffusion through the oxide is the controlling mechanism in this type of oxidation: the process has been studied extensively and is rather well understood (Ref. 7).

When the oxidation attack involves alloys (multicomponent metal systems) and includes the simultaneous processes of vaporization and spallation, the situation becomes very complex. Unfortunately, this is usually the case encountered in practice for alloys developed to possess specific high temperature mechanical properties. If the oxide formed has a sufficiently high vapor pressure or if the oxide further oxidizes to form a volatile species, metal can be transported from the oxidizing component by the volatile oxide species. This type of attack generally manifests itself as a weight loss and for some systems it has been studied extensively (e.g., Ref. 8). In addition

ORIGINAL PAGE IS
OF POOR QUALITY

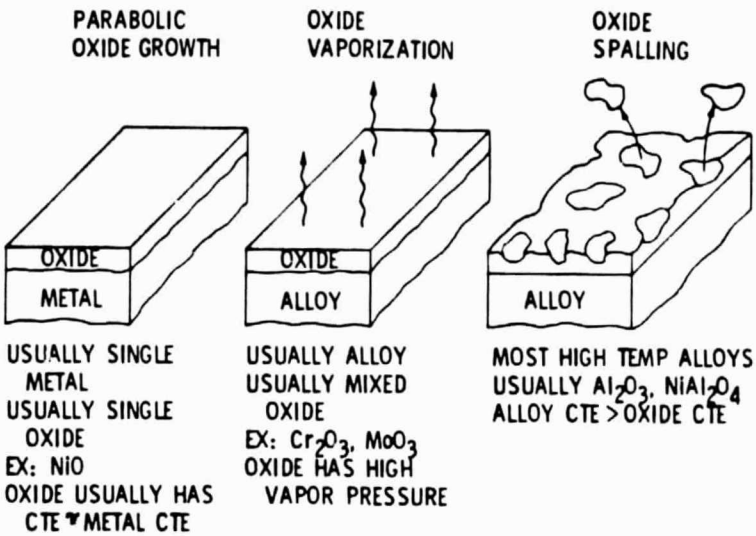

Figure 3. Schematic representations of modes of oxidation attack (CTE-coefficients of thermal expansion).

to oxide growth and vaporization, spallation can contribute to overall oxidation attack. Spallation also results in a net weight loss of the component, but the mechanisms of this type of attack are not well established. Because spallation is often associated with thermal cycling, it is viewed as the result of a mismatch in the coefficients of thermal expansion of the metal and the oxide (Refs. 9, 10).

The specific weight changes characteristic of some modes of oxidation attack are represented in figure 4. Parabolic oxide growth rate behavior is characterized by the rate constant K_p. The combination of parabolic oxide growth and linear vaporization oxide loss results in a net paralinear behavior which can be characterized by a combination of K_p and the vaporization rate constant K_v. Finally, when spalling is also included, still another rate constant, K_s, must be added to characterize the behavior. The spallation rate constant, K_s, represents the linear type of spallation weight loss approached at long times. The dashed line shown in figure 4 is the resultant actually observed in laboratory cyclic oxidation tests (Ref. 9). The stepped curve represents schematically what happens on each heating-cooling cycle. During each heating cycle, new oxide forms and possibly simultaneously vaporizes to some extent; on cooling, weight is lost as oxide spalls.

Actual weight change curves measured for a number of advanced gas turbine engine airfoil materials are shown in figure 5. These advanced materials were cyclically tested at 1100°C

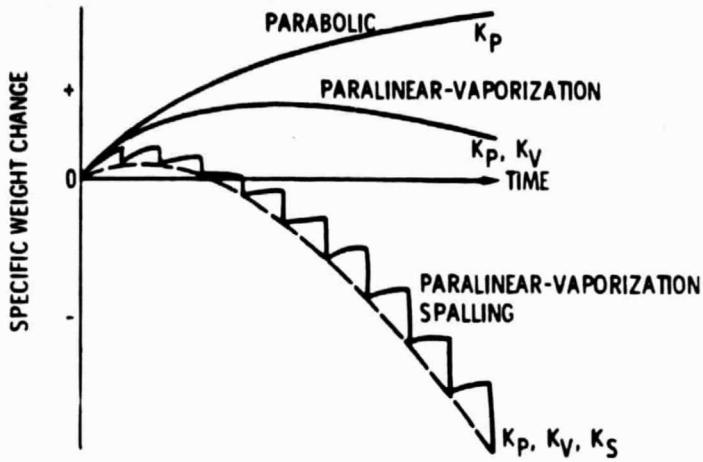

Figure 4. Specific weight changes with time for major modes of oxidation attack.

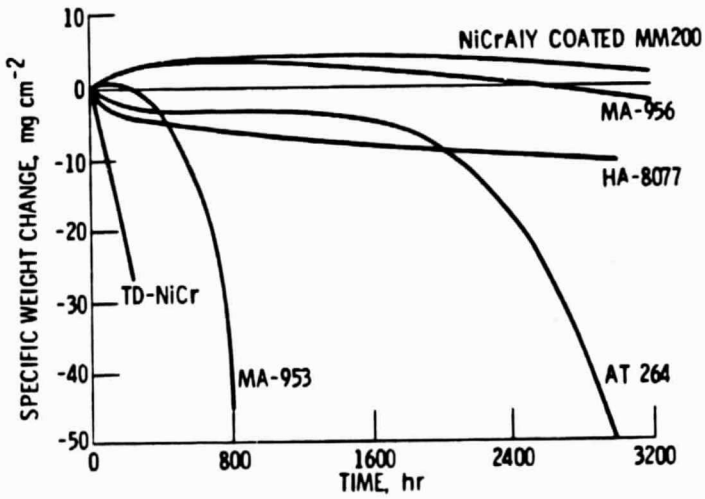

Figure 5. Cyclic oxidation results obtained in Mach 0.3 burner rig. Metal temperature was 1100°C; one hour at temperature per cycle.

in a Mach 0.3 burner rig burning Jet A fuel. The large weight losses observed for TD-NiCr and MA-953 result from vaporization. These two alloys form a chromia (Cr_2O_3) scale which further oxidizes to CrO_3. At high temperatures, CrO_3 readily vaporizes in a high velocity gas stream. Chromium is thus transported away from the alloy to produce a rapid weight loss

and ultimately the integrity of the alloy is compromised. The NiCrAlY-coated MM-200 forms a predominately aluminum oxide (Al_2O_3) scale which does not vaporize and the observed slight weight loss is due to spalling. The iron-chromium-aluminum alloy, MA-956, likewise shows good oxidation resistance while the other two materials undergo considerable spallation and show significant weight losses at intermediate times. Metallographic examination of these oxidized materials show microstructures that reflect the levels of their respective weight losses, figure 6. The NiCrAlY-coated MM-200 and MA-956 show generally minor surface attack with only isolated regions showing more severe attack in the former. On the other hand, the HA-8077 shows considerable attack with many voids widespread throughout the material (Ref. 11).

From the above examples, one can see that it is far more desirable to have some ability to predict oxidation attack rather than to perform tests that require thousands of hours. Except for some single metals which follow simple oxide growth

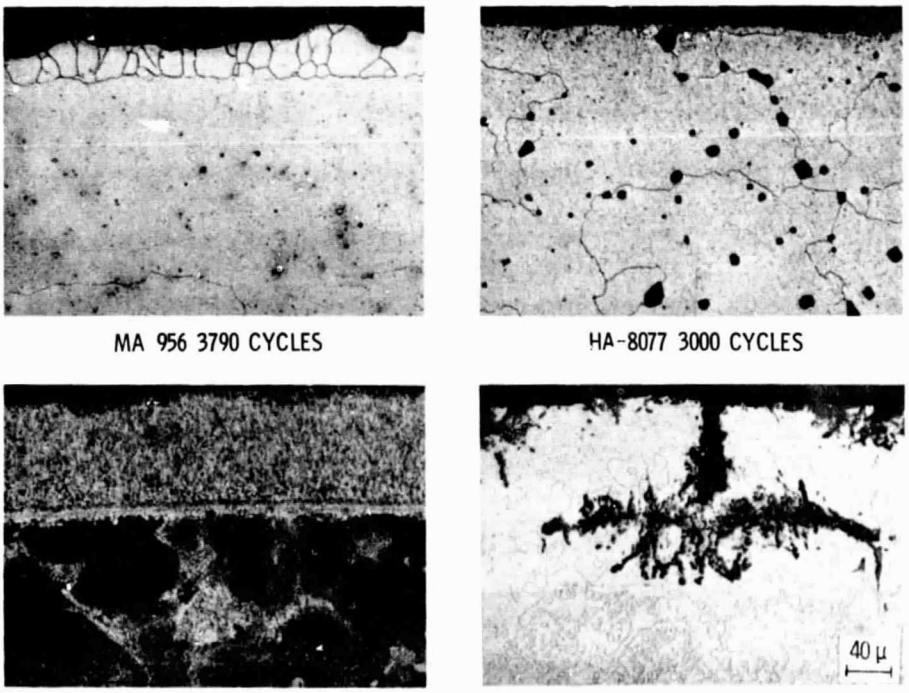

MA 956 3790 CYCLES

HA-8077 3000 CYCLES

NiCrAlY COATED MM200 AS RECEIVED

NiCrAY COATED MM200 3790 CYCLES

Figure 6. Microstructures of materials tested in cyclic oxidation. Metal temperature was 1100°C; one hour at temperature per cycle.

ORIGINAL PAGE IS
OF POOR QUALITY

rate kinetics, there have been relatively few attempts to predict long term oxidation attack. At the NASA-Lewis Research Center, we have been addressing this problem. The parabolic oxidation attack equation has been extended to a more generalized attack prediction scheme (Refs. 12, 13). This approach relates specific weight change to mechanisms of attack by the equation

$$\frac{\Delta W}{A} = (K_p t)^{1/2} - K_v t - K_s t \pm \sigma$$

where ΔW is weight change, A is surface area, K_i is the respective rate constant, t is time and σ is an error parameter. Data from short time laboratory tests are fitted to this equation by regression analysis. If there is a satisfactory fit of the data (of 33 oxidation resistant alloys, only two were found to be anomalous (Ref. 14)), then the data are entered into a

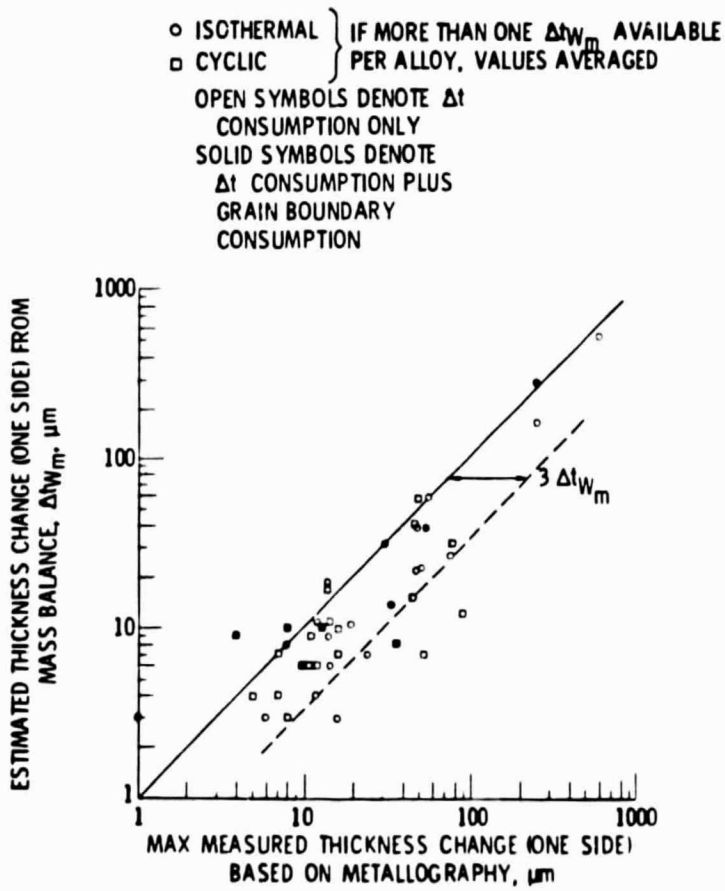

Figure 7. COREST estimated versus measured metal thickness loss for 100 hours cyclic oxidation at metal temperature of 1150°C and one-hour cycles.

computer program called COREST 9 (Ref. 11) to analyze and extrapolate the oxidation behavior. COREST is based on a material balance approach where information on the oxide scale composition is used to calculate the average effective thickness of metal lost. Figure 7 is a comparison of COREST predicted thickness losses with measured values for numerous alloys tested cyclically at 1150°C. It is to be noted that the measured values are those for maximum attack while the COREST values are estimates of average attack. The predicted values are seen to be within at least a factor of three of measured values and this demonstrates that our ability to predict oxidation attack is progressing.

We have also used the above technique in a program aimed at developing more oxidation resistant alloys. The results presented in figure 8 show iso-attack contours on ternary phase diagrams for a series of Ni-Cr-Al alloys (Ref. 13). The values indicated on the contour lines are a measure of the degree of oxidation attack and lower numbers indicate increased oxidation resistance. The contours, for materials melted in ZrO_2 crucibles, indicate that at 1200°C best cyclic oxidation weight change resistance is obtained for the compositions Ni45Al and Ni35Cr15Al. The first composition was expected because it is in the β-phase region typical of the widely used aluminide coatings used for superalloy protection. The second composition however was only identified by the present approach. Another interesting feature is shown by comparison of the two diagrams in figure 8. For the alloys where Zr was added by melting in ZrO_2 crucibles, spalling resistance was increased. Apparently the Zr promotes an increase in the oxide-metal bond.

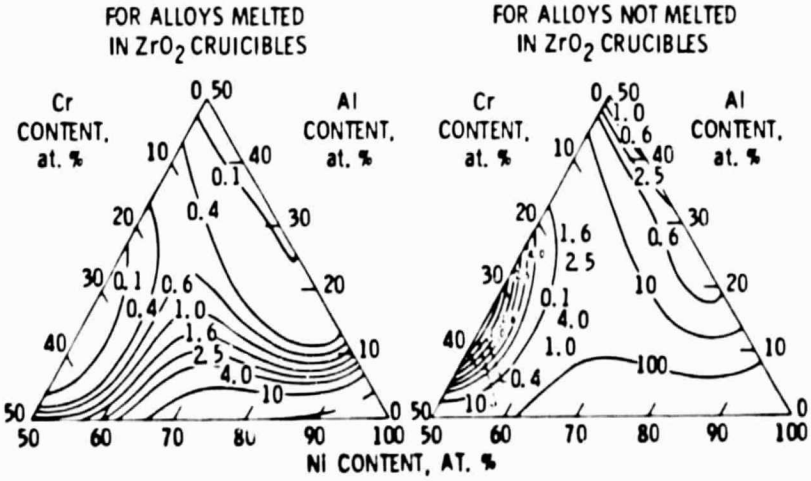

Figure 8. Attack contours for Ni-50Cr-50Al system at 1200°C.

The foregoing indicates that our ability to predict oxidation attack continues to develop. Spallation, the most common form of weight loss, is now predicted by the NASA approach. While current predictions are not as accurate as desired, this methodology is maturing. Problems associated with alloy surface depletion and changing oxide scale composition are still to be solved before reliable long time predictions can be made with confidence.

Hot Corrosion and Other Impurity Effects

Impurities or contaminants which enter the high temperature system can cause a number of different kinds of environmental attack of components. In gas turbine engines, operating on quite pure fuels, it is not uncommon for the fuel to contain trace quantities of elements such as sulfur and vanadium as impurities. Air ingested into the engine can contain varying amounts of such airborne substances as sand and sea salt aerosol (composition approximately 69% NaCl, 15% $MgCl_2$, 11% Na_2SO_4, 3% $CaCl_2$, and 2% KCl). These various "impurities" can undergo chemical reaction in the combustion process to form other compounds which subsequently exit the combustor along with the fuel-air combustion products. Metal components at high temperatures which are subject to the flow of these materials from the combustor can undergo environmental attack beyond that of oxidation.

Some types of environmental attack associated with impurity effects are represented very schematically in figure 9. Certain gaseous species can react with or otherwise compromise the integrity of the normally self-limiting (protective) oxide developed on alloy components (Refs. 14, 15). Once the pro-

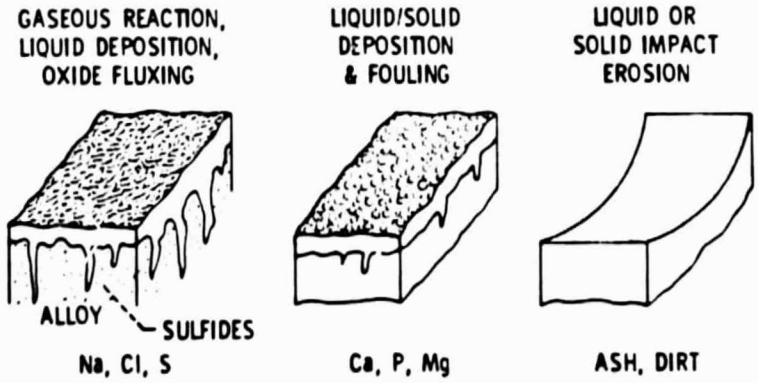

Figure 9. Schematic representations of environmental attack.

ORIGINAL PAGE IS
OF POOR QUALITY

tective oxide is compromised, bare metal surface is exposed which can be further attacked. Certain compounds that deposit on components as liquids can also compromise the oxide and attack the substrate to produce hot corrosion and sulfidation attack (Refs. 17, 18, 19). Compounds containing the elements Na, V, S, and Cl have been identified as contributing to the above modes of attack. Deposition of other chemically less aggressive substances causes other harmful effects like cooling hole plugging and fouling of aerodynamic configurations. These harmful effects are also classified as attack and they are generally associated with compounds containing the elements Ca, P, Fe, and Mg (Ref. 5). Erosion attack results from the direct mechanical removal of component material by impact of hard substances like ash, sand, or dirt.

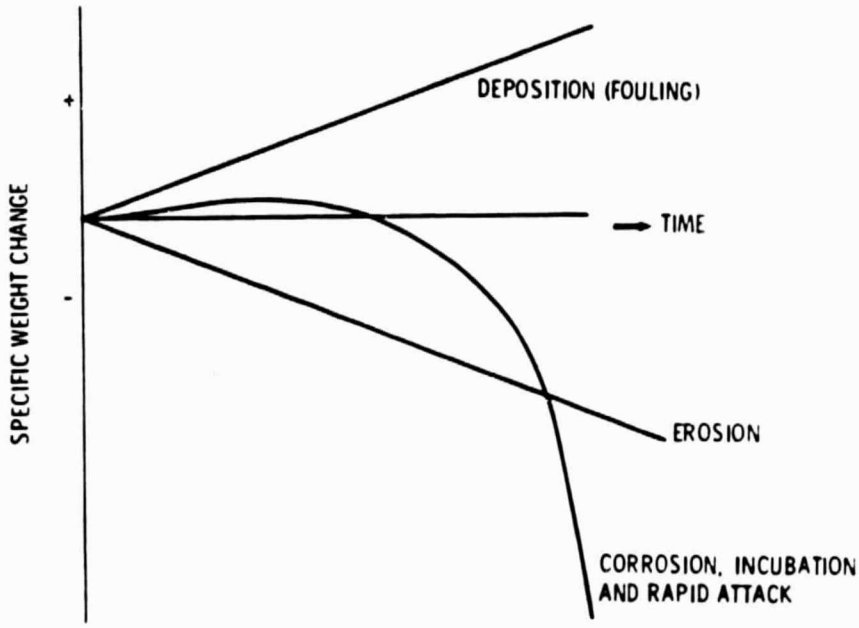

Figure 10. Specific weight changes for three modes of "impurity" associated environmental degradation.

The weight change behaviors associated with these types of environmental attack are indicated in figure 10. Of course in actual service, it is probable that several of these types of attack take place simultaneously. As expected, deposition/fouling is manifested as a weight gain. This attack can be sporadic and it is not catastrophic to components although it can reduce airflow through the gas turbine and cause engine stall. Mechanismwise, deposition is expected to be related

to the chemistry of formation of compounds in the combustion process, dew points, mass transport rates, and possibly nucleation. No systematic approach has yet been applied to developing a predictive capability for deposition/fouling attack.

Erosion attack always results in a weight loss. The attack is generally quite linear in time although it may be sporadic. Mechanistically one would expect this mode of attack to be relatively uncomplicated, but little has been done to develop an ability to predict high temperature erosion of the type illustrated in figure 11 (Ref. 20).

ORIGINAL PAGE IS
OF POOR QUALITY

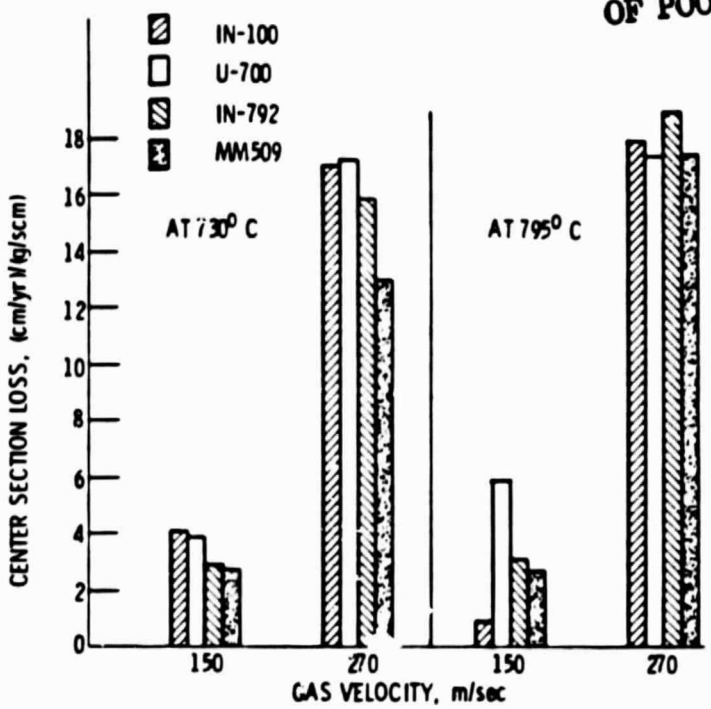

Figure 11. Erosion of turbine alloys in the effluent of a pressurized fluidized bed.

As was indicated in figure 10, hot corrosion attack is catastrophic in that once initiated, it proceeds very rapidly in time. Catastrophic attack is proceeded by an incubation period of unpredictable and varying duration during which very little weight change takes place. Of all the modes of attack associated with impurity effects, hot corrosion is unquestionably the most complicated mechanistically.

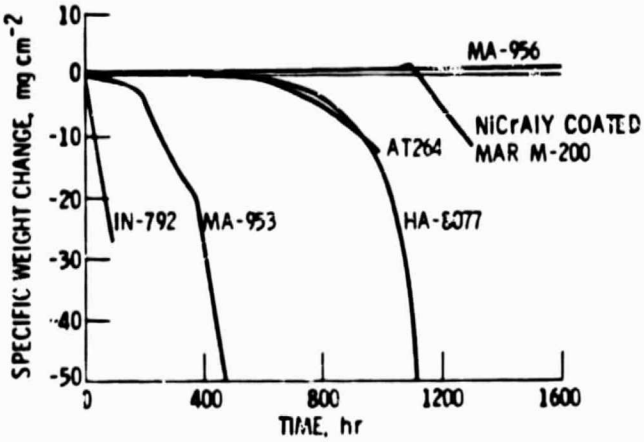

Figure 12. Cyclic hot corrosion results obtained in Mach 0.3 burner rig: 5 ppm synthetic sea salt aqueous solution added to combustor; 900°C metal temperature; one hour at temperature per cycle.

A few weight change examples reflecting hot corrosion attack are presented in figure 12. These results were obtained in a burner rig hot corrosion test which is basically similar to a cyclic oxidation burner rig test except that a synthetic sea salt aqueous solution is continually added into the combustion chamber. At a metal test temperature of 900°C, the oxidation behavior of the materials in figure 12 is known to be good, but the weight losses indicate that all except the MA-956 sustained an unexceptable amount of hot corrosion attack (Ref. 11). Post test metallographic examination of the test samples likewise indicated severe attack for all except the MA-956 which showed only minimal damage. Typically observed microstructures are shown in figure 13.

The severity of hot corrosion attack has provided the impetus for much research in many laboratories in the United States and England (Ref. 21). At the NASA-Lewis Research Center, there has been a continuing effort to (1) characterize the phenomena, (2) understand the mechanisms involved, and (3) alleviate the hot corrosion problem. Basic research has been directed at determining the chemistry and kinetics of corrosive salt formation in combustion systems. Doped laboratory flames have been investigated by high pressure mass spectrometric sampling techniques (Refs. 3, 22). These studies have established that sodium sulfate, considered the primary salt responsible for hot corrosion attack (Refs. 4, 17, 18), is formed in

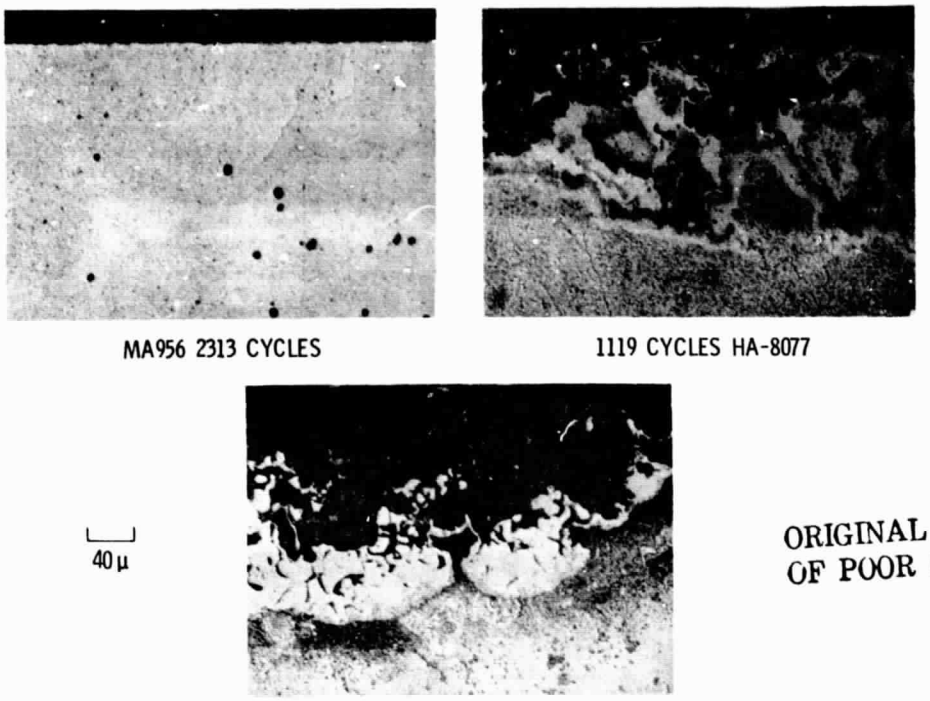

ORIGINAL PAGE IS
OF POOR QUALITY

Figure 13. - Microstructures of oxidation resistant materials after hot corrosion tests. 900^{0} C; 5 ppm sea salt; 1 hr/cycle; X250.

Figure 13. Microstructures of materials tested in cyclic hot corrosion. Metal temperature was 900°C; one hour at temperature per cycle; 5 ppm synthetic sea salt.

flames doped with sodium-containing salts and sulfur compounds (Ref. 23). The time required for formation of the sulfate is very short ($<$ 1 millisecond) compared to the residence time in gas turbine engines and therefore the observed flame chemistry is applicable to real engines. Typically measured composition profiles for a particular laboratory flame system are compared with equilibrium thermodynamically calculated compositions in figure 14. The agreement shown between measured and calculated compositions is satisfactory enough to establish that equilibrium calculations can be applied to other aspects of the hot corrosion problem.

Equilibrium calculations have been used to determine dew points for sodium sulfate and other compounds as a function of various burner rig and engine parameters (Ref. 2). Calculated condensation temperatures have been found to be in good agreement with measured values (Ref. 24) and a transport theory is being developed to predict deposition rates. This is considered to be the first step toward the objective of ultimately being able to predict attack rates. The present state of

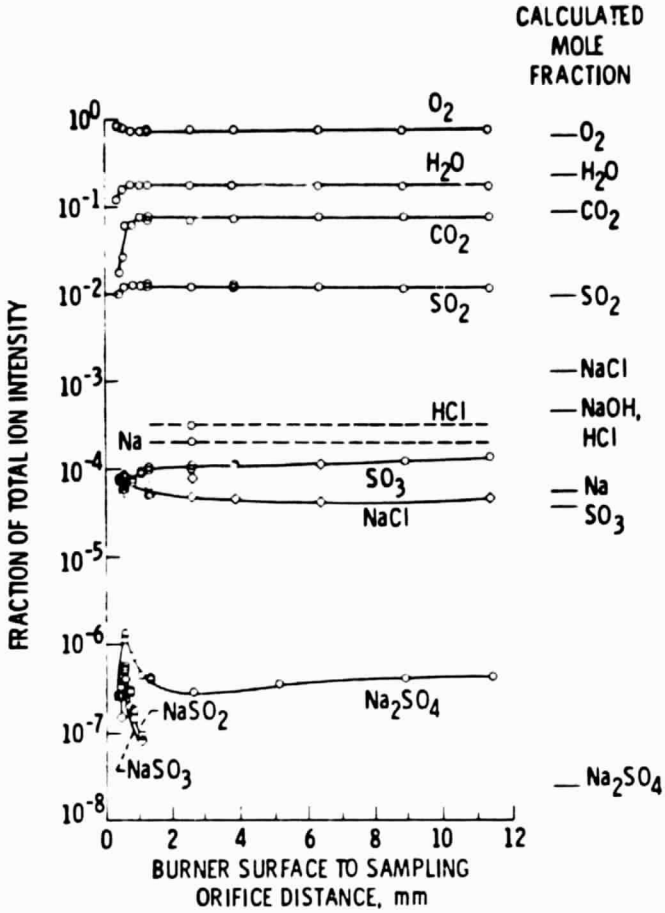

Figure 14. Measured composition profiles and calculated compositions for doped flame. Reactants (wt %): CH_4 = 4.7, O_2 = 89.4, H_2O = 3.5, SO_2 = 2.0, and NaCl = 0.35.

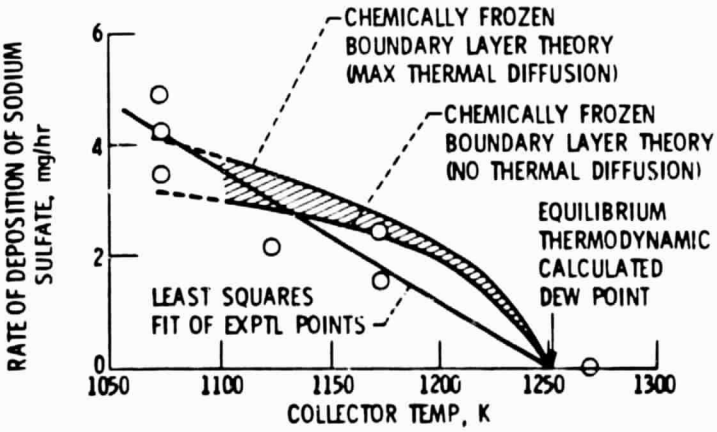

Figure 15. Comparison of experimentally measured and theoretically calculated deposition rates of Na_2SO_4 from burner rig (Mach 0.3) flame doped with 8 ppm NaCl.

ORIGINAL PAGE IS
OF POOR QUALITY

development of our predictive approach is indicated in figure 15. While calculated and measured dew points are seen to be in good agreement, theoretical rate predictions are not yet in satisfactory agreement with measurements. However, these initial results have provided valuable insights into the hot corrosion process and are considered encouraging enough to justify further work to refine the transport theory.

Solutions to the hot corrosion problem can be sought semi-empirically in (1) improved alloys or ceramics, (2) protective surface coatings, (3) use of additives to the engine environment, and (4) air/fuel cleanup to eliminate harmful impurities. A number of these approaches are being pursued at the NASA-Lewis Research Center. For example, figure 16 shows the reduction in hot corrosion attack that can be attained by heavily doping a highly hot corrosive test environment with a chromium type fuel additive (Ref. 25). Other additives are also being evaluated, but because of considerations of price, logistics, etc., additives are not deemed to be the ultimate solution to the hot corrosion problem.

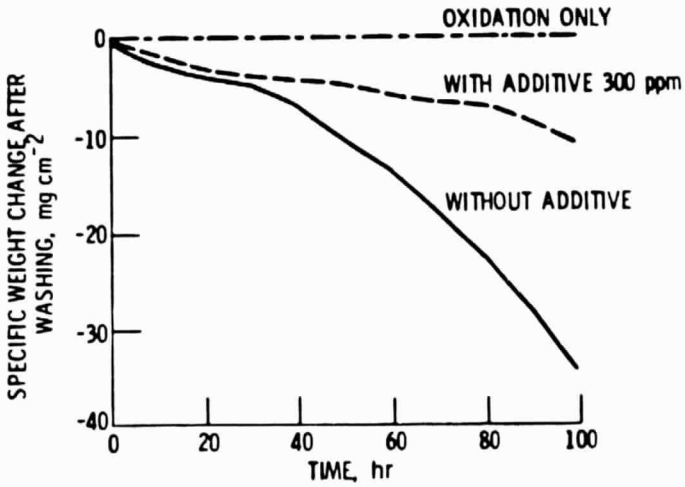

Figure 16. Effect of chromium additive on cyclic hot corrosion; Mach 0.3 burner rig; 900°C metal temperature; one hour at temperature per cycle; 5 ppm synthetic sea salt.

As gas turbine engines (and other power systems) are operated on more impure fuels, such as the type characterized in table I, the hot corrosion problem is expected to increase in severity. With more impurities, one can expect increases in the complexity of (1) the reactions involved, (2) the effects of additives, and (3) the trade-offs in alloy and coating compositions.

TABLE I

TYPICAL RESIDUAL OIL TRACE ELEMENT CONCENTRATIONS

	ppm		ppm		ppm
S	12,000	Na	35	Pb	2
Si	300	Cl	2	Zr	2
V	180	Ba	4	Rb	2
Fe	150	Zn	4	Nd	1
Ni	120	P	4	Y	1
Ca	120	Cr	3	Se	1
K	80	Co	3		
Al	75	Mn	2.5		
Mg	75	Cu	2.5		

CONCLUDING REMARKS

In attempting to summarize the current status of understanding of environmental attack, one is faced with areas in which good progress has already been made and areas in which much more remains to be done. In the former category is oxidation. The ability to understand and predict the effects of oxidation, especially cyclic oxidation, has grown rapidly in recent years. Hot corrosion in relatively "clean" fuel systems is farther behind; the mechanisms are becoming clear but our predictive capabilities are still in their infancy. Erosion and deposition, while presumably more straightforward, are only beginning to be considered. Finally, our understanding of the effects of all the impurities found in "dirty" fuels, e.g. residual oils and some coal-derived liquids, is in the very earliest development stages and this area offers many chanllenges.

REFERENCES

1. D. A. Spera and S. J. Grisaffe, NASA TM X-2664 (1973).

2. F. J. Kohl, C. A. Stearns, and G. C. Fryburg, in "Metal-Slag Gas Reactions and Processes," Ed. by Z. A. Foroulis and W. W. Smeltzer, The Electrochemical Society Soft Bound Series, p. 649 (1975). Also, NASA TM X-71641 (1975).

3. C. A. Stearns, R. A. Miller, F. J. Kohl, and G. C. Fryburg, J. Electrochem. Soc., 124, (7), 1145 (1977). Also NASA TM X-73600 (1977).

4. J. Stringer, "Hot Corrosion in Gas Turbines," MCIC Rpt. 72-08 (1972).

5. D. L. Deadmore and C. E. Lowell, NASA TM X-73661 (1977).

6. Committee on Conservation of Materials Through Reduction of Erosion, Erosion Control in Energy Systems, NMAB-334 (1977).

7. K. Hauffe, "Oxidation of Metals," Plenum Press, N.Y. (1965).

8. C. S. Tedmon, J. Electrochem. Soc., 113, (8), 766 (1966).

9. C. A. Barrett and C. E. Lowell, Oxidation of Metals, 9, (4), 307 (1975).

10. D. L. Deadmore and C. E. Lowell, Oxidation of Metals, 11, (2), 95 (1977).

11. C. E. Lowell and D. L. Deadmore, NASA TM X-73656 (1977).

12. C. A. Barrett and A. F. Pressler, NASA TN D-8132 (1976).

13. C. A. Barrett and C. E. Lowell, Oxidation of Metals, 11, (4), (1977).

14. C. A. Barrett, Proceedings of Conference on Environmental Degradation of Engineering Materials, Oct. 10-12, 1977, College of Engineering, Virginia Polytechnical Institute and State University, Blacksburg, VA, pp. 319-327 (1977).

15. C. A. Stearns, F. J. Kohl, and G. C. Fryburg, NASA TM X-73467 (1976).

16. G. C. Fryburg, R. A. Miller, F. J. Kohl, and C. A. Stearns, NASA TM X-73599 (1977). Also, J. Electrochem. Soc., 124, (11), 1738 (1977).

17. J. A. Goebel, F. S. Pettit, and G. W. Goward, Met. Trans., 4, (1), 261 (1973).

18. N. S. Bornstein, M. A. DeCrescente, and H. A. Roth, Met. Trans. 4, (8), 1799 (1973).

19. C. A. Stearns, F. J. Kohl, and G. C. Fryburg, NASA TN D-8461 (1977).

ORIGINAL PAGE IS
OF POOR QUALITY

20. G. R. Zellars, A. P. Rowe, and C. E. Lowell, "Corrosion/Erosion of Turbine Blade Materials in the High-Velocity Effluent of a Pressurized Fluidized Coal Combustor," Fifth International Conference of Fluidized-Bed Combustion, Dec. 12-14, 1977, Washington, DC.

21. Proceedings of Third Conference on Gas Turbine Materials in a Marine Environment, University of Bath, England, Sept. 20-23, 1976.

22. C. A. Stearns, F. J. Kohl, G. C. Fryburg, and R. A. Miller, NASA TM-73720 (1977).

23. G. C. Fryburg, R. A. Miller, C. A. Stearns, and F. J. Kohl, NASA TM-73794 (1977).

24. F. J. Kohl, G. J. Santoro, C. A. Stearns, G. C. Fryburg, and D. E. Rosner, NASA TM X-73683 (1977).

25. C. E. Lowell and D. L. Deadmore, NASA TM X-73465 (1976).